ACS APPLIED MATERIALS & INTERFACES

Letter

www.acsami.org

Hyperbranched Quasi-1D TiO_2 Nanostructure for Hybrid Organic–Inorganic Solar Cells

Ali Ghadirzadeh,[†,‡] Luca Passoni,[†,§] Giulia Grancini,[†] Giancarlo Terraneo,[∥] Andrea Li Bassi,[†,‡] Annamaria Petrozza,[†] and Fabio Di Fonzo*[,†]

[†]Center for Nanoscience and Technology @PoliMi, Istituto Italiano di Tecnologia, Via Giovanni Pascoli 70/3, 20133 Milano, Italy

[‡]Dipartimento di Energia, Politecnico di Milano, Via Ponzio, 20133 Milano, Italy

[§]Dipartimento di Fisica, Politecnico di Milano, Piazza L. Da Vinci 32, 20133 Milano, Italy

[∥]Laboratory of Nanostructured Fluorinated Materials (NFMLab), Department of Chemistry, Materials, and Chemical Engineering "Giulio Natta", Politecnico di Milano, Milan, Italy

Supporting Information

ABSTRACT: The performance of hybrid solar cells is strongly affected by the device morphology. In this work, we demonstrate a poly(3-hexylthiophene-2,5-diyl)/TiO_2 hybrid solar cell where the TiO_2 photoanode comprises an array of tree-like hyperbranched quasi-1D nanostructures self-assembled from the gas phase. This advanced architecture enables us to increase the power conversion efficiency to over 1%, doubling the efficiency with respect to state of the art devices employing standard mesoporous titania photoanodes. This improvement is attributed to several peculiar features of this array of nanostructures: high interfacial area; increased optical density thanks to the enhanced light scattering; and enhanced crystallization of poly(3-hexylthiophene-2,5-diyl) inside the quasi-1D nanostructure.

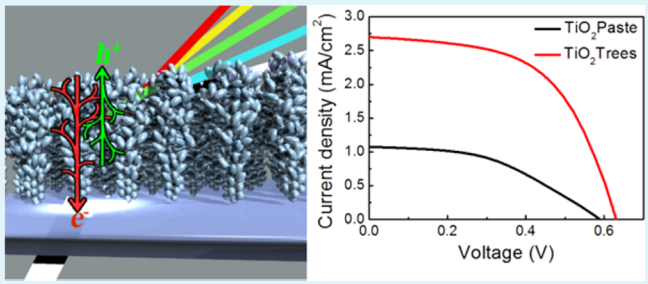

KEYWORDS: *hyperbranched nanostructures, hybrid solar cells, pulsed laser deposition, P3HT, 1D nanostructures, self-assembled*

Hybrid solar energy devices (HSC) comprise a high band gap n-type metal oxide nanostructure, commonly TiO_2, and a light-absorbing conjugated polymer functioning as hole-transporting material.[1−3] Upon light illumination, photo-induced excitons are generated in the organic material and charge separation takes place at the organic−inorganic interface where electrons are injected into the inorganic semiconductor.[4,5] The morphology of the active layer strongly affects the performance of hybrid devices, and thus proper engineering of the organic−inorganic heterojunction remains a key issue in developing hybrid solar cells.[6−8] The key features for an efficient device are (i) high interfacial area between the acceptor and the donor materials in order to increase the active area for charge separation; (ii) continuous pathways for the separated charges in order for them to reach the electrodes and avoid recombination in lattice traps and defects; (iii) organic domains with dimensions not exceeding in size the exciton diffusion length, which is on the order of 5−20 nm. The most common approach[9,10] consists of blending inorganic nanocrystals with an organic conjugated polymer. Despite this simple method, which achieves a high interfacial area, presents issues related to blend inhomogeneity and instability of the mixture, which over time leads to a disordered matrix with little control over the polymer domain size. Although efficient charge separation is eased by a large interfacial area, exciton migration to the interface is hampered by large polymer domains and charge collection is prevented by the random blend network. HSC based on the TiO_2/Poly(3-hexylthiophene-2,5-diyl) (i.e., TiO_2/P3HT) blend have not been able to reach a power conversion efficiency higher than 0.5%.[11] An alternative solution is to use one-dimensional nanostructures such as nanowires[12] or nanotubes[13] that provide preferential carrier pathways, thus reducing charge recombination.[14,15] A further advantage of 1D structures is the potential for increasing polymer crystallinity by enhancing alignment of P3HT chains along their structures. As demonstrated by K.M Coakley et al., a 20-fold increase in hole mobility can be achieved in crystallized P3HT molecules infiltrated in ordered nanotubes.[16] A power conversion efficiency close to 1% has been achieved,[17] but the modest specific surface area has kept this approach far away from the ideal structure. An different approach to induce ordering of the polymer at the interface with TiO_2 is the use of molecular interlayers, as reported by some of the coauthors of this work[18] increasing power conversion efficiency from 0.37 to 0.95%. Although a comparative table is provided in the Supporting Information, a complete review on the perform-

Received: December 22, 2014
Accepted: March 30, 2015
Published: March 30, 2015

DOI: 10.1021/am5090429
ACS Appl. Mater. Interfaces 2015, 7, 7451−7455

ances of different hybrid devices can be found in the literature.[19]

In our previous work,[20] hierarchical TiO_2 nanostructures were modeled by high-angle annular dark-field scanning transmission electron microscopy (HAADF-STEM) tomography to gain insight into their 3D structure. Monotonic connectivity, defined as the ratio of the titanium dioxide in contact with the electrodes through a decreasing path length, was found to be 0.89 when considering the bottom electrode versus 0.69 when considering the top contact. Such geometrical asymmetry in the titanium dioxide structures is thought to favor electron transport toward the anode, reducing the recombination rate of photogenerated charges. Geometrical tortuosity of the hierarchical structure, defined as the ratio between the length of the shortest charge collection path divided by the orthogonal distance along the *z*-axis, was also analyzed. The average values were found to be 1.466 and 1.559 toward the anode and in the opposite direction respectively (comparable to literature values ranging from 1.0 to 2.0).[21,22] These values are also the evidence that the directional morphology of these structures is facilitating electron transport toward the anode. Further analysis in the presence of infiltrated P3HT showed that over 75% of the polymer volume is within 8.5 nm of the interface crucial for a high rate of exciton collection. A prototype nonoptimized hybrid solar cell with an efficiency of 0.66% was reported as an example. The optimization of the pulsed laser deposition allowed for the fabrication of a complex film morphology comprising an array of quasi-1D hyperbranced nanostructures with high specific surface area and directional porosity along the film thickness. This nanoarchitecture, previously shown to work as an efficient photoanode in liquid and solid DSSC,[23,24] indeed presents an interconnected network with open channels and high specific surface area. Quasi-1D hyperbranched nanostructures, thanks to their size being in the range of the wavelength of visible light, act as integrated Mie scattering elements diffusing the transmitted light and enhancing the device optical thickness eventually improving light absorption and photogenerated current (as reported in other works).[25] For the fabrication of such nanostructures, pulsed laser deposition is performed inside a vacuum chamber in the presence of a background gas. In a certain range of deposition parameters, multidirectional cluster scattering is induced so that an array of quasi-1D hierarchical nanostructures grows directly from the gas phase perpendicular to the substrate. The film thickness is a function of laser energy and increases linearly with deposition time. The film porosity, specific surface area, and pore diameter characteristics of the nanostructures are a function of the deposition pressure and annealing temperature. The as deposited films are amorphous and are typically annealed at 500 °C for 2 h in air to achieve the anatase crystalline phase. This allotropic phase is well-known to optimize charge injection and transport as well as the maximal specific surface area requirements. As reported in previous publications, film possessing a given density, upon thermal treatment, shows preferential crystal growth along the [004] direction forming hyperbranched nanostructures, sometimes referred to as nanotrees.[24,26] Through TEM and X-ray diffraction analysis it was demonstrated that among the annealed samples deposited at different pressures, those deposited at an O_2 pressure of 7 Pa were optimal for obtaining a hyperbranched structure with a crystal domain size of several tens of nanometers along the *c* direction [004].[24] An example of the hyperbranched assembly is presented in Figure 1. Here

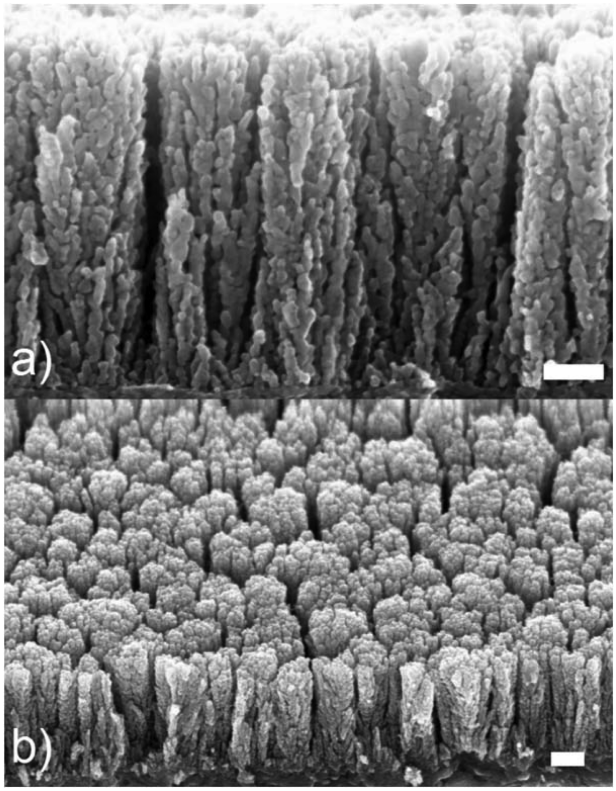

Figure 1. Crystalline hyperbranched TiO_2 deposited at 7 Pa Oxygen pressure; (a) cross-sectional view; (b) tilted view showing both cross-section and top surface of the hyperbranched nanostructures. Scale bar: 100 nm.

we show how optimized quasi-1D hyperbranched nanostructure self-assembled from the gas phase by PLD (deposited in 7 Pa of O_2) enhances the photovoltaic performance in hybrid organic solar cells when compared to standard mesoporous/P3HT devices (see methods in Supporting Information for details on material and device fabrication and characterization). To be consistent with the above-mentioned published work,[18] we used the optimized reference architecture found there as a benchmark throughout this study. In HSCs, the morphology of the nanostructured photoanode must comprise pores sufficiently large and interconnected to allow continuous polymer infiltration and, at the same time, polymer domains smaller than the exciton diffusion length to impede exciton recombination. Using Brunauer–Emmett–Teller (BET) technique, it was shown that a low deposition pressure resulted in a low porosity (high density) and low specific surface area film, while a high deposition pressure resulted in a high porosity (low density) and high specific surface area.[24] It should be noted that for a photoanode composed of hyperbranched structures, the polymer must infiltrate into a complex hierarchical void path. Although nanometric voids (spaces between braches) fulfill the dimensional requirements imposed by the exciton diffusion length, in the case of films with excessive porosity the micrometric channels among 1D hyperbranched nanostructures are thought to be responsible for polymer accumulation in domains big enough (>50 nm) to hamper exciton diffusion and thus charge separation.[27] In Figure S1 in the Supporting Information, the optical transmittance for the films with different porosities infiltrated with P3HT is reported to demonstrate that a larger amount of infiltrated polymer is present in the more porous structures

DOI: 10.1021/am5090429
ACS Appl. Mater. Interfaces 2015, 7, 7451–7455

(i.e., lower transmittance). The effect of film thickness is investigated on films ranging from 0.1 to 2 μm showing the best results for an 800 nm thick film (Figure S2 in the Supporting Information) and it is compared to the average and maximum performance of control devices comprising a nanoparticle-based photoanode., fabricated following the protocol reported in previous work.[18] The number of charge recombination sites is increased in thinner film by polymer accumulation and in the case of thicker films by the excessive length of the electron path. Indeed, the series resistance is found to be minimized for 800 nm thick samples deposited at 7 Pa, whereas increases for both thinner and thicker devices can be seen in Figure S3 in the Supporting Information.

For devices based on the hyperbranched photoanode (h-PA), an average power conversion efficiency of 0.8%, exceeding 1% for the best device, is recorded. Performance of the optimized h-PA devices, are compared with a standard mesoporous structure prepared using a titanium dioxide nanoparticle paste mixed with the same polymer. The $J-V$ curves of champion devices can be found in Figure 2 where a greater than 2 fold

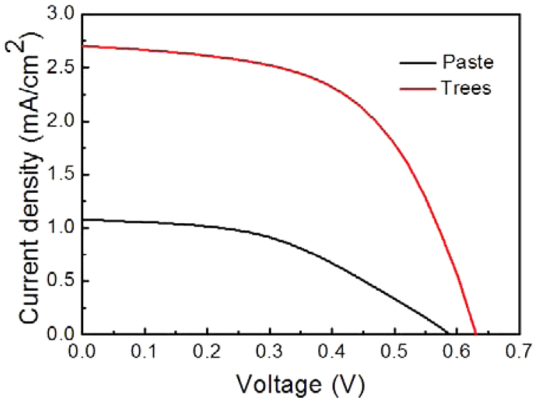

Figure 2. Performance comparison between devices comprising hyperbranched photoanode and standard mesoporous photoanode.

increase in performance (PCE = 1% and PCE = 0.34% for the h-PA device and the standard device respectively) mainly due to the enhancement in photogenerated current (2.7 mA/cm^2 and 1.15 mA/cm^2 for the h-PA device and the standard device respectively) is reported. This 130% current density improvement is in the first instance attributed to light scattering in the hyperbranced nanostructure increasing the device optical thickness and enhancing its light-harvesting efficiency. The optical characterization of the devices was performed both on crystalline mesoporous and hyperbranched optimized photoanodes before and after P3HT infiltration. Figure S4 in the Supporting Information shows a schematic illustration of the comparison between the mesoporous structure (a) and the hierarchical nanostructure (b).

Whereas the total transmittance and the haze factor can be found in the Supporting Information (Figure S5), Figures 3a shows the diffuse transmittance curves for both structures, with and without P3HT. The hyperbranced photoanode, in comparison to the one with standard nanoparticles, shows significantly higher diffuse transmittance indicating higher light scattering. This behavior can be explained by the fact that h-PAs are composed of arrays of nanotrees with a characteristic longitudinal size of the same order of magnitude as the incident light. Acting as scattering elements, these structures enhance the photoanode optical thickness, increasing the photon

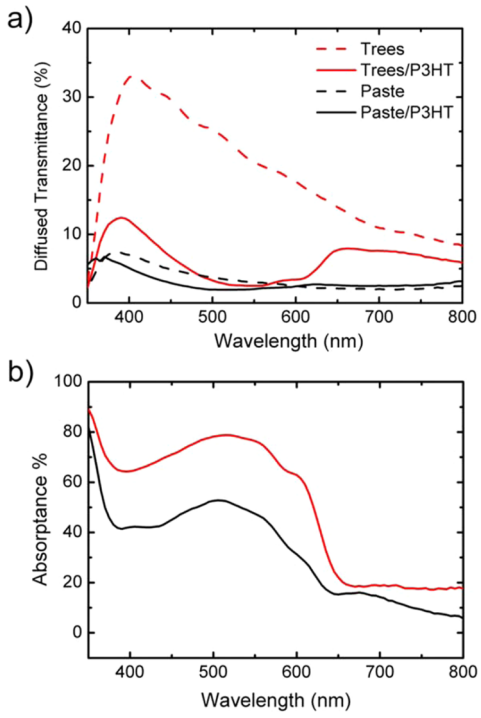

Figure 3. Optical characterization curves for the optimized h-PA device (red) in comparison to standard mesoporous structure (black): (a) diffused transmittance, (b) absorptance of TiO_2/P3HT.

interaction with the photoactive layer therefore enhancing the PCE. As can be seen in Figure 3a, scattering increases in the spectral range around 450 nm, which is the wavelength for which the characteristic size of quasi-1D hyperbranched nanostructure presents a higher scattering cross-section. In Figure 3b, absorptance curves are presented showing an increase of optical density for a hyperbranched structure when compared to standard mesoporous nanoparticles. Over the visible range an average absorptance increase of +60% in the h-PA devices can be observed in comparison with a standard nanoparticle-based device. The absorbance curve of P3HT over the hyperbranched nanostructure differs from that of the mesoporous paste. If normalized (Figure S6 in the Supporting Information), it becomes evident that for the h-PA device, an increase in the 380–430 nm range arises as a consequence of the strong scattering that characterizes this spectral region. Interestingly, a higher relative intensity for wavelengths around 630 nm is also observed. The latter phenomenon could be ascribed to a more intense vibronic structure resulting from a higher molecular order in the polymer[28,29] when infiltrated into the quasi-1D nanostructure rather than into the mesoporous film. To further study the effect of the inorganic scaffold on polymer crystallinity, X-ray diffraction is used and results are reported in Figure 4a. The analysis has been performed on scaffolds with and without the polymer capping layer (SEM images of the cross-sections of these samples are reported in Figure S7 in the Supporting Information). In the presence of a capping layer the strong peak at 2θ= 5.4°, related to the (100) plane of crystalline P3HT, is present despite the nature of the scaffold. On the other hand, when the polymer is only present in the oxide scaffold, only the 1D hyperbranched structures show crystalline phases. To relate this structural information to the operation of the solar cell, we have performed time-resolved pump probe on a time window

DOI: 10.1021/am5090429
ACS Appl. Mater. Interfaces 2015, 7, 7451–7455

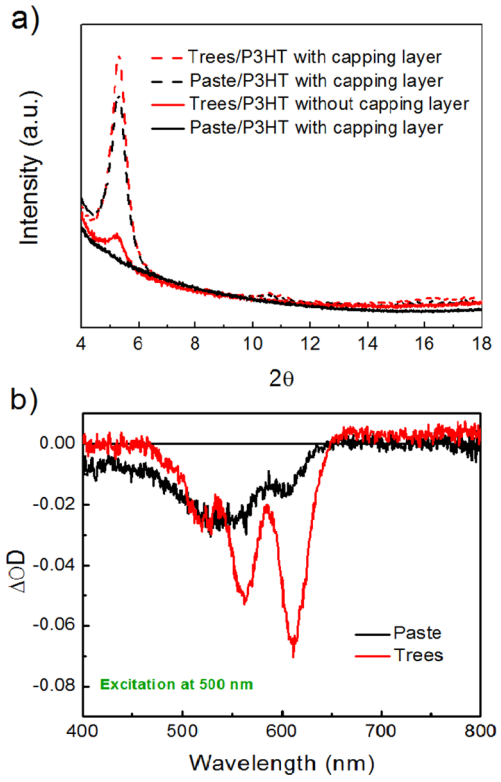

Figure 4. Evidence for P3HT crystallinity. Hyperbranched structures (red) and mesoporous nanoparticle paste (black): (a) XRD spectra of the films with P3HT capping layer (dashed line) and without P3HT capping layer (solid line) and (b) nanosecond transient absorption.

of hundreds of nanoseconds, when long-living charge carriers represent the main photoexcited population. Differential absorption spectra integrated in the first 500 ns upon excitation at 500 nm for the P3HT/trees (red) and P3HT/paste (black) samples are displayed in Figure 4b. The spectra reveal a negative signal in the 450−620 nm region that is due to P3HT photobleaching (PB) in good agreement with the absorption spectrum. The PB band at this time scale is related to charges. The polymer deposited on the h-PA photoanode shows a much more resolved structure of the photobleaching with a high relative intensity of the vibronic peaks.[30] On the other hand, the P3HT infiltrated into TiO_2 paste shows a blue-shifted absorption and a less pronounced vibronic structure. As it is well-known that these optical features are correlated to specific morphological characteristics of the conjugated polymer, i.e., to crystalline phases in the first case, disordered/amorphous phases in the latter, we can conclude that in the presence of 1D hyperbranched nanostructures, photocarriers are mainly moving along ordered crystalline structures that can sustain higher carrier mobility and lower recombination processes at the interface.[30,31] Moreover, considering that in a complete device structure the polymer capping layer over the scaffold tends to reach a higher level of order (thus a smaller band gap), independently of the nature of the layer underneath, the possibility of also achieving a long-range order in the bulk reduces the degree of energetic disorder in the device that would affect the harvesting of photogenerated excitons away from the interface and the collection of carriers.

In this work, we demonstrated the fabrication of a quasi-1D hyperbranched nanostructure of TiO_2, self-assembled from the gas phase by means of pulsed laser deposition and its successful application as a photoanode in hybrid organic−inorganic solar cells. Self-assembled quasi-1D hyperbranched nanostructures were coupled with P3HT in a hybrid solar cell. A power conversion efficiency of 1% was achieved. Such a result originates from an increase in photogenerated current as a consequence of the higher optical thickness of h-PA devices induced by strong light scattering. Moreover, devices comprising quasi-1D hyperbranched nanostructures could also benefit from fast electron transport, high interfacial area between the polymeric and inorganic phases, and from P3HT molecular ordering.

■ ASSOCIATED CONTENT

Ⓢ Supporting Information

Total transmittance of film at different porosity, device thickness optimization, devices series resistance, optical analysis, SEM cross-section of P3HT infiltrated films. This material is available free of charge via the Internet at http://pubs.acs.org.

■ AUTHOR INFORMATION

Corresponding Author

*E-mail: fabio.difonzo@iit.it. Tel. +39 0223999868.

Notes

The authors declare no competing financial interest.

■ ACKNOWLEDGMENTS

We acknowledge James Ball for help in revising the manuscript.

■ REFERENCES

(1) Weickert, J.; Auras, F.; Bein, T.; Schmidt-Mende, L. Characterization of Interfacial Modifiers for Hybrid Solar Cells. *J. Phys. Chem. C* **2011**, *115*, 15081−15088.

(2) Boucle, J.; Ravirajan, P.; Nelson, J. Hybrid Polymer−Metal Oxide Thin Films for Photovoltaic Applications. *J. Mater. Chem.* **2007**, *17*, 3141−3153.

(3) Zhang, G.; Finefrock, S.; Liang, D.; Yadav, G. G.; Yang, H.; Fang, H.; Wu, Y. Semiconductor Nanostructure-Based Photovoltaic Solar Cells. *Nanoscale* **2011**, *3*, 2430−2443.

(4) Weickert, J.; Dunbar, R. B.; Hesse, H. C.; Wiedemann, W.; Schmidt-Mende, L. Nanostructured Organic and Hybrid Solar Cells. *Adv. Mater.* **2011**, *23*, 1810−1828.

(5) Zhou, R.; Xue, J. Hybrid Polymer-Nanocrystal Materials for Photovoltaic Applications. *ChemPhysChem* **2012**, *13*, 2471−2480.

(6) Chen, W.; Nikiforov, M. P.; Darling, S. B. Morphology Characterization in Organic and Hybrid Solar Cells. *Energy Environ. Sci.* **2012**, *5*, 8045−8074.

(7) Gur, I.; Fromer, N. A.; Chen, C.-P.; Kanaras, A. G.; Alivisatos, A. P. Hybrid Solar Cells with Prescribed Nanoscale Morphologies Based on Hyperbranched Semiconductor Nanocrystals. *Nano Lett.* **2007**, *7*, 409−414.

(8) Iza, D.; Muñoz-Rojas, D.; Musselman, K.; Weickert, J.; Jakowetz, A.; Sun, H.; Ren, X.; Hoye, R.; Lee, J.; Wang, H.; et al. Nanostructured Conformal Hybrid Solar Cells: a Promising Architecture Towards Complete Charge Collection and Light Absorption. *Nanoscale Res. Lett.* **2013**, *8*, 1−9.

(9) Wright, M.; Uddin, A. Organic-Inorganic Hybrid Solar Cells: A Comparative Review. *Sol. Energy Mater. Sol. Cells* **2012**, *107*, 87−111.

(10) Chandrasekaran, J.; Nithyaprakash, D.; Ajjan, K. B.; Maruthamuthu, S.; Manoharan, D.; Kumar, S. Hybrid Solar Cell Based on Blending of Organic and Inorganic Materials-an Overview. *Renewable Sustainable Energy Rev.* **2011**, *15*, 1228−1238.

(11) Coakley, K. M.; McGehee, M. D. Photovoltaic Cells Made from Conjugated Polymers Infiltrated into Mesoporous Titania. *Appl. Phys. Lett.* **2003**, *83*, 3380−3382.

DOI: 10.1021/am5090429
ACS Appl. Mater. Interfaces 2015, 7, 7451−7455

(12) Zhang, Q.; Yodyingyong, S.; Xi, J.; Myers, D.; Cao, G. Oxide Nanowires for Solar Cell Applications. *Nanoscale* **2012**, *4*, 1436−1445.
(13) Wisnet, A.; Thomann, M.; Weickert, J.; Schmidt-Mende, L.; Scheu, C. Nanoscale Investigation on Large Crystallites in TiO_2 Nanotube Arrays and Implications for High-Quality Hybrid Photodiodes. *J. Mater. Sci.* **2012**, *47*, 6459−6466.
(14) Yu, K.; Chen, J. Enhancing Solar Cell Efficiencies Through 1-D Nanostructures. *Nanoscale Res. Lett.* **2009**, *4*, 1−10.
(15) Sato, K.; Dutta, M.; Fukata, N. Inorganic/Organic Hybrid Solar Cells: Optimal Carrier Transport in Vertically Aligned Silicon Nanowire Arrays. *Nanoscale* **2014**, *6*, 6092−6101.
(16) Coakley, K. M.; Srinivasan, B. S.; Ziebarth, J. M.; Goh, C.; Liu, Y.; McGehee, M. D. Enhanced Hole Mobility in Regioregular Polythiophene Infiltrated in Straight Nanopores. *Adv. Funct. Mater.* **2005**, *15*, 1927−1932.
(17) Wu, M. C.; Chang, C. H.; Lo a, H. H.; Lin, Y. S.; Lin, Y. Y.; Yen, W. C.; Su, W. F.; Chen, Y. F.; Chen, C. W. Nanoscale Morphology and Performance of Molecular-Weight-Dependent Poly(3-hexylthiophene)/TiO_2 Nanorod Hybrid Solar Cells. *J. Mater. Chem.* **2008**, *18*, 4097−4102.
(18) Canesi, E. V.; Binda, M.; Abate, A.; Guarnera, S.; Moretti, L.; D'Innocenzo, V.; Sai Santosh Kumar, R.; Bertarelli, C.; Abrusci, A.; Snaith, H.; et al. The Effect Of Selective Interactions at the Interface of Polymer-Oxide Hybrid Solar Cells. *Energy Environ. Sci.* **2012**, *5*, 9068−9076.
(19) Wright, M.; Uddin, A. Organic—Inorganic Hybrid Solar Cells: a Comparative Review. *Sol. Energy Mater. Sol. Cells* **2012**, *107*, 87−111.
(20) Divitini, G.; Stenzel, O.; Ghadirzadeh, A.; Guarnera, S.; Russo, V.; Casari, C. S.; Bassi, A. L.; Petrozza, A.; Di Fonzo, F.; Schmidt, V.; et al. Nanoscale Analysis of a Hierarchical Hybrid Solar Cell in 3D. *Adv. Funct. Mater.* **2014**, *24*, 3043−3050.
(21) Kroese, D. P.; Brereton, T.; Taimre, T.; Botev, Z. I. Why the Monte Carlo Method is so Important Today. *Comput. Stat.* **2014**, *6*, 386−392.
(22) Thiedmann, R.; Stenzel, O.; Spettl, A.; Shearing, P. R.; Harris, S. J.; Brandon, N. P.; Schmidt, V. Stochastic Simulation Model for the 3D Morphology of Composite Materials in Li-ion Batteries. *Comput. Mater. Sci.* **2011**, *50*, 3365−3376.
(23) Sauvage, F.; Di Fonzo, F.; Li Bassi, A.; Casari, C. S.; Russo, V.; Divitini, G.; Ducati, C.; Bottani, C. E.; Comte, P.; Graetzel, M. Hierarchical TiO_2 Photoanode for Dye-Sensitized Solar Cells. *Nano Lett.* **2010**, *10*, 2562−2567.
(24) Passoni, L.; Ghods, F.; Docampo, P.; Abrusci, A.; Martí-Rujas, J.; Ghidelli, M.; Divitini, G.; Ducati, C.; Binda, M.; Guarnera, S.; et al. Hyperbranched Quasi-1D Nanostructures for Solid-state Dye-sensitized Solar Cells. *ACS Nano* **2013**, *7*, 10023−10031.
(25) Lin, J.; Heo, Y.-U.; Nattestad, A.; Yamauchi, Y.; Dou, S. X.; Kim, J. H. Mesoporous Hierarchical Anatase for Dye-sensitized Solar Cells Achieving Over 10% Conversion Efficiency. *Electrochim. Acta* **2015**, *153*, 393−398.
(26) Jun, Y.; Casula, M. F.; Sim, J.; Kim, S. Y.; Cheon, J.; Alivisatos, A. P. Surfactant-Assisted Elimination of a High Energy Facet as a Means of Controlling the Shapes of TiO_2 Nanocrystals. *J. Am. Chem. Soc.* **2003**, *125*, 15981−15985.
(27) Divitini, G.; Abrusci, A.; Fonzo, F. D.; Snaith, H.; Ducati, C. Quantitative Electron Tomography Investigation of a TiO_2 Based Solar Cell Photoanode. *J. Phys.: Conf. Ser.* **2014**, *522*, 012063.
(28) Hintz, H.; Egelhaaf, H. J.; Luer, L.; Hauch, J.; Peisert, H.; Chasse, T. Photodegradation of P3HT-a Systematic Study of Environmental Factors. *Chem. Mater.* **2011**, *23*, 145−154.
(29) Brown, P. J.; Thomas, D. S.; Köhler, A.; Wilson, J. S.; Kim, J.; Ramsdale, C. M.; Sirringhaus, H.; Friend, R. H. Effect of Interchain Interactions on the Absorption and Emission of Poly(3-hexylthiophene). *Phys. Rev. B* **2003**, *67*, 064203.
(30) Guo, J.; Ohkita, H.; Benten, H.; Ito, S. Charge Generation and Recombination Dynamics in Poly(3 hexylthiophene)/Fullerene Blend Films with Different Regioregularities and Morphologies. *J. Am. Chem. Soc.* **2010**, *132*, 6154−6164.
(31) Guo, J.; Ohkita, H.; Benten, H.; Ito, S. Near-IR Femtosecond Transient Absorption Spectroscopy of Ultrafast Polaron and Triplet Exciton Formation in Polythiophene Films with Different Regioregularities. *J. Am. Chem. Soc.* **2009**, *131*, 16869−16880.

DOI: 10.1021/am5090429
ACS Appl. Mater. Interfaces 2015, 7, 7451−7455